Desalination and Water Treatment
www.deswater.com

doi: 10.1080/19443994.2015.1076738

57 (2016) 14647–14655
July

Taylor & Francis
Taylor & Francis Group

Synthesis, characterization, and photocatalytic activity of TiO_2–SiO_2 nanocomposites

Hossein Ijadpanah-Saravi[a], Mehdi Zolfaghari[b], Ahmad Khodadadi[c], Patrick Drogui[b,*]

[a]*Faculty of Engineering, Department of Environmental Engineering, Tarbiat Modares University, Tehran, Iran, Tel. +98 9303162646; email: hossein.ijad@gmail.com*
[b]*Institut National de la Recherche Scientifique (INRS-ETE), Université du Québec, 490 rue de la Couronne, G1K 9A9 Quebec City, Quebec, Canada, Tel. +1 418 654 2530, ext. 4446; Fax: +1 418 654 2600; email: mehdi.zolfaghari@ete.inrs.ca (M. Zolfaghari), Tel. +1 418 654 3119; Fax: +1 418 654 2600; email: patrick.drogui@ete.inrs.ca (P. Drogui)*
[c]*Environmental Engineering, and Head of Modares Environmental Research Center (MERC), Tarbiat Modares University, Nasr Bridge, Tehran, Iran, Tel. +98 21 82883399; Fax: +98 2188006544; email: akdarban@modares.ac.ir*

Received 7 December 2014; Accepted 11 June 2015

ABSTRACT

Introduction of complex chemical compounds in the wastewater treatment plants challenged the biological process efficiency. Photocatalyst oxidation was newly introduced to remove the trace organic contaminations. Since their surface area determined the production of hydroxyl radicals, the pure TiO_2 surface area was increased by the preparation of TiO_2–SiO_2 nanocomposite using sol–gel technique. Later on, the X-ray diffraction, scanning electron microscopy, energy diffraction spectroscopy, Fourier transform infrared spectroscopy, UV–vis reflective dispersion spectroscopy, and adsorption of nitrogen gas were deployed for its characterization. Anatase phase was detected as the dominant form of nanocomposites made in this study. Furthermore, rise of calcination temperature, increased the nanoparticle pore size. Therefore, 600˚C was selected to gain the optimum nanoparticle pore size (around 10 nm). Finally, the photocatalytic activities of the synthesized nanoparticles were evaluated for removing Acid Blue 9 (AB9) dye. The photocatalytic performance of the most optimized ratio TiO_2–SiO_2 nanocomposites was three times higher than that of pure TiO_2 and even commercial nanoparticle.

Keywords: TiO_2 nanoparticles; TiO_2–SiO_2 nanocomposites; Sol–gel method; Photocatalysis; Dye removal

1. Introduction

Disposal of synthetic dyes from different industries such as textile, food, paper, printing, cosmetics, pharmaceutical, petrochemical, agriculture, and tannery into municipal and industrial wastewater treatment plants has led to various severe environmental problems [1]. Conventional biological processes face challenge to remove those complex aromatic base compounds [2–4]. Discharge of trace concentration of residual dyes not only has toxic effect on aquatic life, but also prevents light penetration and interrupts photosynthesis process. Moreover, recent regulations on dye disposal put pressure on these industries to meet the allowable concentrations before disposal of

---

*Corresponding author.

effluents [1]. In this regard, finding effective methods such as adsorption, oxidation, and enzymatic decomposition is a vital and inevitable issue [5].

Because of its capability to react quickly with trace organic contaminants in wastewater, the hydroxyl radical produced by advance oxidation processes (AOPs) were the most studied method for dye removal worldwide. Because of its diverse energy band gap, stability, and cheapness, nano-TiO_2, especially the anatase phase, has widely utilized in photocatalytic oxidation processes [1,6–10]. Direct relation between expose surface area to light and the photocatalytic performance demanded the application of the powder photocatalytic in slurry reactors due to its high surface area (up to 300 m^2/g) [9,11]. However, weak adsorption capacities of those photocatalysts powder, recycling, and low diffusion of radiation are their main disadvantages.

On the other hand, immobilized photoreactors suffer from lower external mass transfer area, replacement of carrier [4], and difficulties in production of uniformed catalyst layer. For making them comfortably reusable, researchers recently were looking for cheap material as the base for the photocatalyst media [12]. Polyurethane [4], Polycarbonate [13], Fe_3O_4 [8], Ag [14], and Pt [3] were examples of bases for SiO_2/TiO_2 photocatalysis in heterogeneous photooxidation. The electron injection of imbedded metal into the surface of catalyst improved its efficiency [14]; however, surface modification will be required to make the nanoparticle matrix free of aggregate [4]. Consequently, fabrication of these multilayers, sensitive, and delicate catalysis are costly, and impractical in industrial scale.

Generally, large energy band gap (3.2 eV) demands higher frequency of light (UV rays with wave length of 387 nm) that result to absorb only 4% of sunrays. N-doped and metal coating titanium largely used to modify the adsorption of greater spectrum of light by photocatalysts [3,14–16]. Combination of TiO_2 with other semiconductors regulating the band gap energy and particles size, minimize, or inhibit charge-carrier recombination, enhancing the thermal and photochemical stability, modifying the surface structure of the photocatalyst by increasing its surface area and porosity, increasing the adsorption level, and their recyclability and reuse [7,10]. Silica (SiO_2) is among the candidate semiconductors for combining with TiO_2, since it provides notable benefits such as transparency, modifying the band gap, increasing the surface area, surface acidity, hydrophilicity, and pore volume. Consequently, it increases the photocatalysis activity, even in darkness [16]. By increasing the surface hydrophilicity, high adsorption of wide range of organic compounds, water, and hydroxyl molecules will be expected [2,7,13,15,17,18]. Finally, addition of silica could inhibit the charge carrier surface recombination, especially in small size particles [19].

The main objective of this work was to investigate feasibility of producing TiO_2–SiO_2 nanoparticles using sol–gel method and tried to modify the method for reaching the maximum anatase phase of TiO_2 nanoparticles and nanocomposites. Then, the synthesized samples were examined for their ability to mineralize a complex compound, Acid Blue 9 (AB9) dye, and optimized the production condition accordingly.

2. Material and method

2.1. Synthesis of nanocatalysts

In this research, TiO_2–SiO_2 nanocomposites were prepared from organic–metallic precursors of titanium tetra isopropoxide (TTIP) and tetra ethyl orthosilicate (TEOS) and their photocatalytic activity was studied in dye removal of C.I. Acid Blue 9, as the model pollutant. Utilization of nitric or oxalic acid instead of hydrochloric acid triggered the formation of anatase phase [12,20]. Distilled water and nitric acid with the ratio of 0.2:150 were mixed, then TEOS was added, and the acidic solution was agitated in a volumetric flask for 1 h at room temperature. In another volumetric flask, isopropanol and ethanol were mixed with the ratio of 1:4 and then TTIP was gradually added and agitated for few minutes which later added to acidic solution. The produced solution was refluxed and the obtained sol was purified and washed with distilled water and ethanol. The remained deposit was dried and calcinated at 400, 500, 600, 700, and 800℃, as those high temperatures require for production of mesostructure [21]. It must be mentioned that, all the materials used in this project had analytical grade and were provided by Merc Co., Germany.

2.2. Measurement of photocatalytic activity

In a 100 ml quartz volumetric flask, 0.1 g of the synthesized photocatalyst was added to 10 mL/L AB9 solution and was exposed to the ultrasonic bath for 15 min for producing a homogenous suspension. Then, this suspension was agitated for 30 min in darkness at room temperature. For reaching the adsorption balance 0.4 mL/min of constant stream of the oxygen gas flowed into the reactor. Finally, after reaching adsorption equilibrium of reactant and suspended catalyst, the solution was exposed to UV light (30 W, $\lambda = 254$ nm, Phillips, Netherland).

The removal of AB9 dye was fitted to the pseudo-first-order kinetic model. Hence, the kinetics of the photocatalyst could be described by the following equation:

$$C = C_0 e^{-kt} \left(t_{1/2} = \frac{\ln 2}{k} \right) \quad (1)$$

where C indicates the AB9 concentration in different time; C_0 is the initial concentration; k is the pseudo-first-order kinetic constant; t is the reaction time; and $t_{1/2}$ is the half-life (min).

2.3. Analytical details

2.3.1. Measurements of the properties of the synthesized nanoparticles

The surface morphology of the TiO_2 photocatalytic material was examined by scanning electron microscopy (SEM, Philips XL-30, FEI Company, Hillsboro, Oregon, USA). The crystallographic structure of the synthetized nanoparticles was characterized by X-ray Diffraction (XRD, Philips xport 1480, Jaarbeurs, Utrecht, Netherlands). The physicochemical surface properties of the nanoparticles were examined using Fourier transform infrared spectroscopy (FT-IR) (Bruker Tensor 27, Munich, Germany). The optical properties of the nanoparticles were measured using UV–vis reflective dispersion spectroscopy (AvaSpec 2048TEC fiber-optic spectrometer, Avantes Company, Beijing China). The physisorption of nitrogen gas (Belsorp min II) was used to evaluate the textural parameter, porosity, and the specific surface of nanoparticles.

2.3.2. Measurements of residual concentration of AB9 dye

The progress of photocatalytic degradation of AB9 dye in solution was firstly monitored by absorbance measurements (absorption peaks previously determined) using a spectrophotometer UV–vis (Ultrospec 2000 UV–visible spectrophotometer, Pharmacia Biotech, Stockholm, Sweden). The UV–vis absorption spectrum of AB9 dye solution was characterized by a peak located in the ultraviolet region. The maximum absorption of the samples had been made at the wavelength of 553 nm in an optical quartz cell (10-mm transmitted path length). Therefore, this absorption peak was chosen to evaluate the residual AB9 dye concentration. A calibration curve (absorbance vs. concentration) was used to calculate the residual AB9 dye concentration.

In order to remove the interrupting effect of dye adsorption on the surface of photocatalyst, for obtaining each data, samples were drawn in the 10 mg/L AB9 solution for 30 min in total darkness; therefore, the removal of dye was just because of photocatalytic reaction.

3. Result and discussion

3.1. Characterization of the photocatalysts

The surface morphology of nanoparticles could determine the efficiency of catalysis. Very fine spherical particle in anatase phase in comparison with large, ragged, and needle shape particle in rutile phase provided higher surface area [20]. According to the SEM images, the particles were spherical with the same topography and pore size. In the first glance, pure TiO_2 nanoparticles obviously had more uniformed and regular morphology compared to TiO_2–SiO_2 nanocomposites. Abundance of macro-crack, and pores in the nanocomposite (Fig. 1(b)) in comparison with the pure nano-TiO_2 (Fig. 1(a)) enabled more active site for substrate adsorption [11]. In Fig. 1(b)

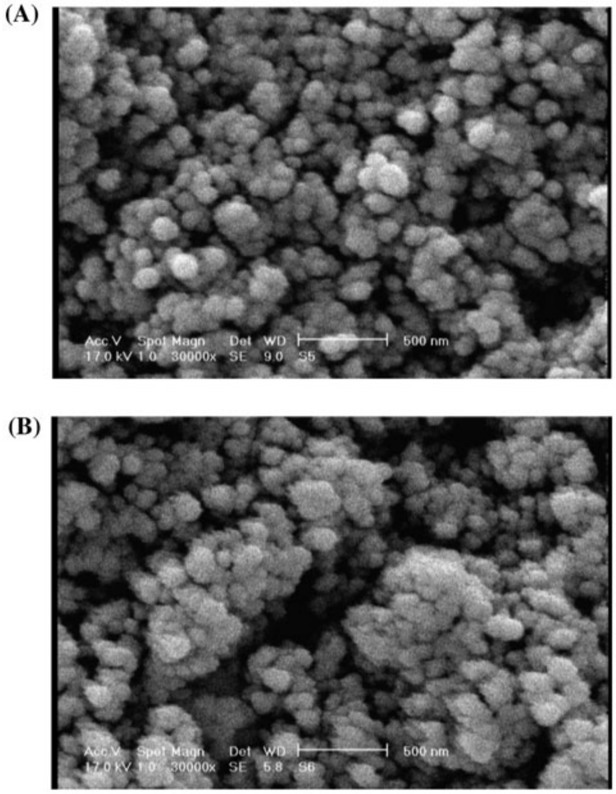

Fig. 1. SEM image of (A) pure nano-TiO_2 and (B) 60% TiO_2–SiO_2 nanocomposite.

the aggregate composed of silica particle was formed rather more homogeneous than TiO_2 particle. Small size nano-TiO_2 was formed on the surface of aggregated silica [21]. In water however, both samples were agglomerated and form massive particles with coarser grain size. Although it reduced the effective surface area, separation of suspended nanoparticle facilitate significantly. It has been reported that agglomerated particle of SiO_2/TiO_2 with the diameter of 200–300 nm could be completely separated by means of decantation in a period of 150 min. Yet, the recovered catalyst activity decrease dramatically (less than half by four times of recovery) because of the aggregate absorption of some organic intermediates [22].

By means of XRD (Fig. 2), pattern and grain size of the pure TiO_2 nanoparticles as well as different ratio of mixture TiO_2–SiO_2 nanocomposites were calculated according to the Debye–Scherer equation (Eq. (2)) [23].

$$D = \lambda\kappa/\beta \cos \theta \tag{2}$$

where D is the mean particle diameter in nm; κ is a constant; λ is X-ray wavelength; and β is width-full width at half maximum in radian; and θ is the angle in which peak was observed. The XRD analysis showed the presence of crystalline TiO_2 nanoparticles embedded inside amorphous silica particles [21]. It seems that the presence of SiO_2 in nanocomposite structure led to particle size reduction. Small size poly-cluster nanoparticles supply enough active site with larger surface area. After the certain limit, the holes and electron become so close to the surface [24]. Therefore, the recombination process rate surpassed the interfacial charge-carrier transfer rate. The results obtained from XRD patterns also revealed that increase in TiO_2/SiO_2 ratio led to thermal stability of the crystallographic structure of TiO_2–SiO_2 nanocomposite, due to the amorphous structure of SiO_2 [25].

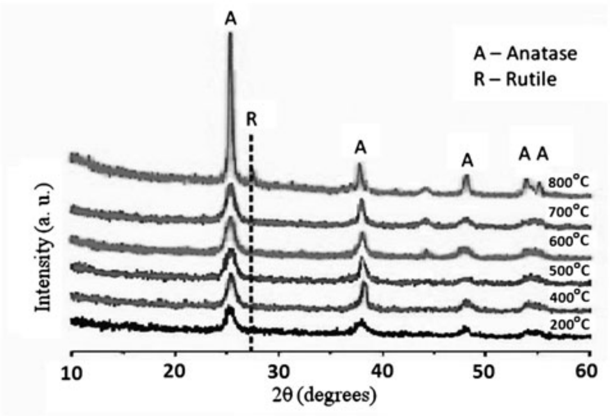

Fig. 2. XRD pattern of the pure TiO_2 nanoparticles and TiO_2–SiO_2 nanocomposites.

The ratio of anatase vs. rutile phase was estimated by Spurr-Meyers equations (Eqs. (3) and (4)):

$$X_A\ (\%) = 100/(1 + 1.265 I_R/I_A) \tag{3}$$

$$X_R\ (\%) = 100/(1 + 0.8 I_A/I_R) \tag{4}$$

where I_A is anatase phase intensity at $2\theta = 25.25^\circ$ [19] and I_R is intensity of rutile peak at $2\theta = 27.42^\circ$, X_R and X_A are terms of weight percentage of anatase and rutile in the sample, respectively. As it illustrated in Fig. 2, rutile peak at $2\theta = 27.42^\circ$ was faintly detectable in comparison with anatase phase. In fact all samples were made up of anatase phase crystalline forms, which was in accordance with previous study by Pinho and Mosquera [21] and Zhang et al. [19].

The result of the ratio of anatase per rutile phase and titanium per silica ratio in different calcination temperature were showed in Table 1. Previous studies stated that the pore volume was decrease by increasing the ratio of pure nano-TiO_2, as its non-porous structure was incorporated with silica gel network [21]. It was also reported that the presence of 5–40% of SiO_2 in nanocomposite significantly reduced the formation of rutile phase, and stabilized the porous structure [2,15]. Presence of anatase phase in the samples made in this study, provided higher density of hydroxyl radical production sites [11,16]. The photocatalyst performance of anatase phase could be fourfold than rutile phase [9].

Table 1 also presents the effect of calcination temperature and TiO_2/SiO_2 ratio on the grain sizes, as those factors are among the most important factor to determine the size of nanoparticles [26]. The calcination temperature of 600℃ generated the optimum size (9.6 nm) of nanocatalysts, which was so closed to the size reported in other studies [7]. Presence of silica in special condition in our study caused the formation of anatase phase even in 800℃. In other researches, the formation of anatase phase was observed at the temperature higher than 550℃ [9], or even in ambient temperature [12]. Our results showed the formation of 100% anatase phase for TiO_2–SiO_2 nanocomposite crystallise was observed (all the sharp peaks were related to the anatase phase) in all temperatures used in this experiment. Like the results of Mahesh et al. [4], the SiO_2 was in amorphous and TiO_2 was in anatase phase. While the anatase phase in other studies was observed at the temperature of 950℃ [2] and 500℃ [16].

Table 1
Grain size and phase structure of the synthesized nanoparticles

Material	Calcination temperature (°C)	Anatase phase percentage (%)	Grain size (nm)
Pure TiO_2	400	100	11.3
60% TiO_2–SiO_2	400	100	7.2
60% TiO_2–SiO_2	500	100	8.1
60% TiO_2–SiO_2	600	100	9.6
60% TiO_2–SiO_2	700	100	11.9
60% TiO_2–SiO_2	800	100	16.4

Calcination temperature escalation may also resulted in the increase in particle size [2]. The particle size increased from 7.2 to 16.4 nm when the calcination temperature rose from 500 to 800°C. The average size of the pure TiO_2 anatase crystallites was estimated to approximately 6.7–11.3 nm. By comparison, the average size of the TiO_2–SiO_2 anatase crystallites was estimated to approximately 7.2 nm for a TiO_2/SiO_2 ratio of 40%.

For the element analysis of the synthesized nanocatalysts, EDS technique was applied in this work. The results obtained from EDS analysis indicated that Ti and Si were well combined with ratios between 58.42% (Ti) and 41.38% (Si) in atomic scale of TiO_2–SiO_2 nanoparticles [2], which was in good agreement with the two values (40 and 60%) used in the synthesis step.

The FT-IR spectrum of the pure TiO_2 nanoparticles and TiO_2–SiO_2 nanocomposite were demonstrated in Fig. 3. Two close peak on Fig. 3(b) in 2θ of 967 and 1,091 cm^{-1} was due to the long chain of high-molecular weight siloxanes that indicate the production of high molecular weight silica polymer by effective sol–gel method. Another reason of the peak on 967 cm^{-1} could be connected to the vibration of Ti–O–Si [21]. The observed peaks of both sample spectra in $2\theta = 642$ and 3,422 cm^{-1} were representative of the tensile resonations of the Ti–O–Ti [15,27] and –OH bonds. The later, attributed to hydroxyl group of water molecules [13]. Moreover, the peak present in $2\theta = 1{,}633$ cm^{-1} was for the bending resonations of the O–H bond of the surface water molecules because of the great hydrophilicity of the SiO_2. Accordingly, the nanocomposite adsorption capability increase for varied hydrophilic and hydrophobic compounds. Also in the FT-IR spectrum of TiO_2–SiO_2 nanocomposites, the observed peak in $2\theta = 1{,}091$ cm^{-1}, was related to the asymmetric resonation of the Si–O–Si nanocomposite (Fig. 4), which is close to previous study with a peak at 1,077 cm^{-1} [12]. Besides, tensile resonations of the asymmetric Ti–O–Si was the most important peak which was located in $2\theta = 957$ cm^{-1}, and confirmed the formation of Ti–O–Si bond, which was a little bit different with the study of Fateh et al. [13] and Mahesh et al. [4] (1,095 and 925 cm^{-1} for Si–O–Si and Ti–O–Si, respectively). This observation proved the interaction between silica and titanium groups that may produce by the reaction of residual silanol and the titanium-bonded isopropyl groups [27]. By the other words, the broad adsorption peak of Si–OH at around 960 cm^{-1} illustrated high surface hydroxyl groups (hydrophilic

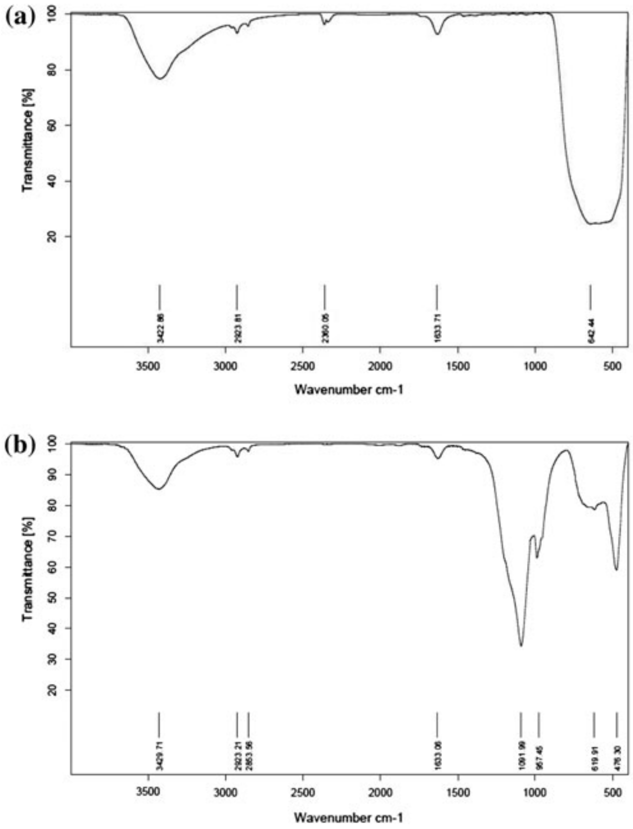

Fig. 3. FT-IR spectrum of: (a) pure TiO_2 nanoparticles, and (b) 60% TiO_2–SiO_2 nanocomposites.

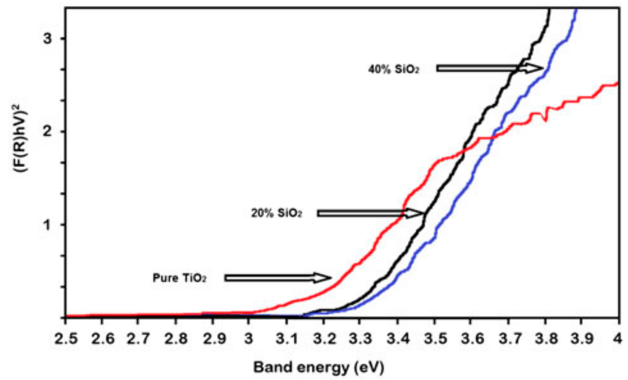

Fig. 4. Determination of band gap energy of the nanocatalysts synthesized through the UV–vis DRS technique.

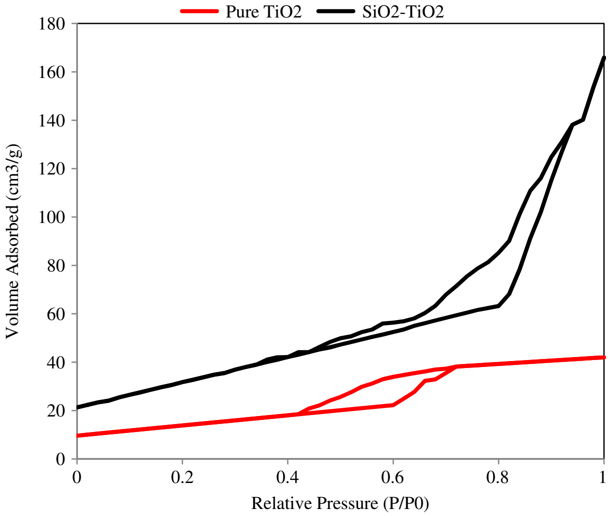

Fig. 5. Adsorption–desorption isotherm of pure TiO_2 nanoparticles and 60% TiO_2–SiO_2 nanocomposites for nitrogen gas.

surface), which increase the potency of hydroxyl radical production [15].

To determine the amount of band gap energy, Kubelka-Munk equation was used (Eq. (5)):

$$F(R) = (1-R)^2/2R = k/s \qquad (5)$$

where $F(R)$ is Kubelka-Munk function; R is reflection; and k and s are absorption and dispersion coefficients of Kubelka-Munk, respectively. As shown in Fig. 4, amount of band gap energy was derived by plotting $(F(R)h\nu)^2$ vs. the photon energy ($h\nu$). The calculated band gap energy for pure TiO_2 nanoparticles was 3.1 eV, which equals to the reported anatase phase band gap [17,28]. By raising the SiO_2 content from 20 to 40 mol%, the band gap energy of nanocomposite increased from 3.33 to 3.35 eV due to the decrease in particle size. By decreasing the particle size in comparison with the pure TiO_2, the adsorption of the visible-light spectrum was decreased; yet, it held forth to have stronger photocatalysis activity [2,15,17]. Expectedly, by increasing in calcination temperature, the band gap energy must be decreased, as the particle size increased. Fig. 5 represents absorption–desorption isotherms of nitrogen on surface of nanocatalysts. The absorption isotherm of both TiO_2–SiO_2 and pure TiO_2 nanoparticles corresponded to isotherms type (IV) of the IUPAC classification indicated the presence of mesoporous materials. Therefore, the adsorption went along by multilayer adsorption and capillary condensation. Capillary condensation caused the steep increase in adsorption for the nanocomposite [29]. The main difference in nanocomposite and pure TiO_2 was about adsorption–desorption hysteresis. Pure TiO_2 exhibited type H1 hysteresis loops which related to the nanoparticles rapidly agglomerate or consist of highly uniform spherical particles [21]. On the other hand, H3 hysteresis loops could be connected to plate-like nanocomposite particles [29]. It also seems that the nanoparticle was more heterogeneous due to dispersion of nano-TiO_2 inside silica matrix. The Brunauer–Emmett–Teller (BET) method used for calculation of specific surface area for pure TiO_2 and TiO_2–SiO_2 nanocomposites which were 45.26 and 105.51 $m^2\ g^{-1}$, respectively. Study of Hou et al. [15] showed larger difference, since the specific surface area were 31.8, 171 and 240 m^2/g for 0, 5 and 30% of SiO_2 in N-dipped TiO_2 [15]. Fig. 6 illustrates pores destitution (BJH) of

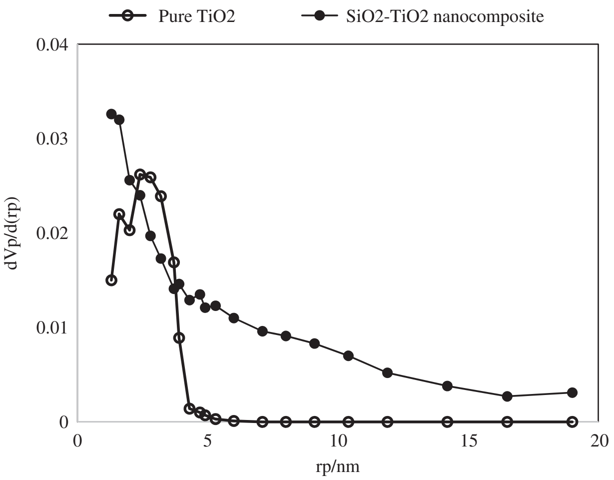

Fig. 6. Pores distribution in pure TiO_2 nanoparticles and 60% TiO_2–SiO_2 nanocomposites.

catalysts surface. The maximum distribution for pure TiO_2 nanoparticles and 60% TiO_2–SiO_2 nanocomposites were 2.8 and 1.3 nm, respectively, implying the pore size reduction with an increase in SiO_2 content, leading to increase the specific surface area of the catalyst. However, the increase in SiO_2 content from 40 to 50% decreased the pore size which was in accordance with the other study [12].

3.2. Decolorization efficiency of the synthetic photocatalyst

In this work, the effect of various molar ratios of TiO_2 to SiO_2, and calcination temperature on catalyst performance reaction was investigated. Ethyl-4-[4-[ethyl-3-sulfophenyl methyl] amino] phenyl ($C_{37}H_{34}N_2Na_2O_9S_3$) with commercial name of Acid Blue 9, wildly used in food and cosmetic industries as a colorant. Because of recalcitrant nature of this highly complex compound in biological process, and easy detection by spectrophotometry method, it was chosen by couple of researchers as an organic contaminant for AOPs [30]. Therefore, in our set of experiments, the removal of AB9 dye was used as an indicator of each different synthetic catalyst performance. Figs. 7 and 8 demonstrated the removal efficiency of photochemical reaction in different irradiation time. According to Fig. 7, synthetic nanocomposites with molar ratio of TiO_2/SiO_2 = 60/40 was chosen as the optimum ratio of those compounds, since further increase or decrease in the ratio had adverse effect on the removal rate of Acid Blue 9 dye. Moreover, the complete mineralization of AB9 dye (more than 99.9% 0f removal) during photooxidation reaction was occurred in less than 24 min of UV radiation (half-life of 2.4 min). For the same immobilized photocatalyst, the total mineralization of Acid Black 1 dye was reported, but in 80 min [4].

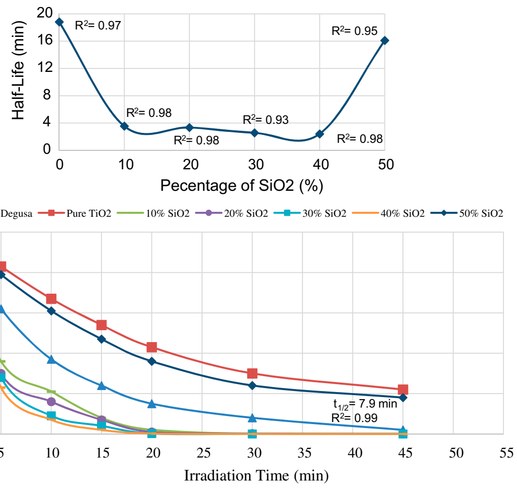

Fig. 7. Effect of the ratio of SiO_2 on the photocatalytic activity of the TiO_2–SiO_2 nanocomposites.

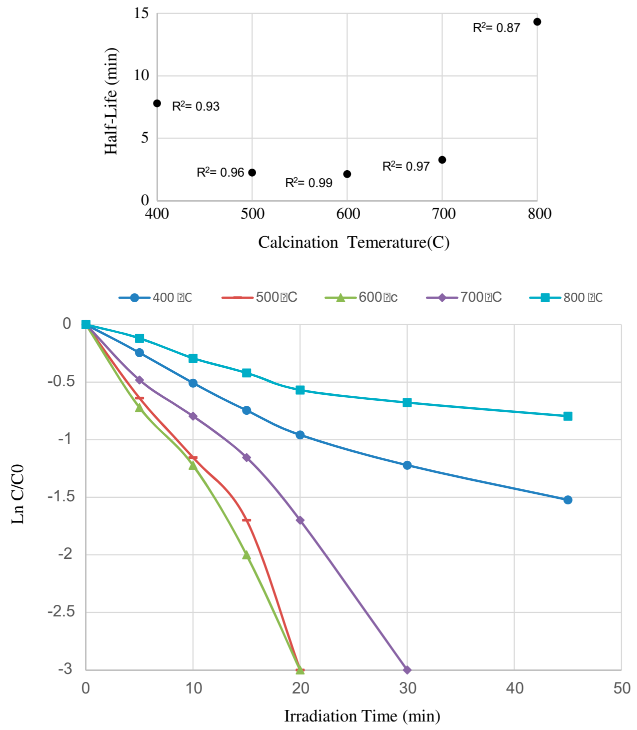

Fig. 8. Effect of calcination temperature on the photocatalytic activity of the TiO_2–SiO_2 nanocomposites for degradation of AB9 (half-life).

The performance of commercial photocatalyst P25 (Degussa company) and common pure TiO_2 nanoparticles for removal of AB9 dye compared by our synthetic photocatalysts in the exactly same operation condition, in order to understand the relative efficiency of the SiO_2–TiO_2 nanocomposite. The results showed that the rate of reaction on the 60% ratio of TiO_2–SiO_2 nanocomposites was 3.3 times faster than commercial photocatalyst P25. The same result was reported for the removal of methylene blue, in which the 10% ratio of TiO_2–SiO_2 increase the removal efficiency from 43 to 66% in comparison with pure TiO_2 [13]. Higher catalysis activity was greatly depended on surface area leading to decline the band gap value, and increase in production of hydroxyl content [6]; therefore, lower grain size of our nanocomposite in comparison to ordinary nano-TiO_2 brought almost eightfold of removal rate. Changing the isoelectric point of TiO_2 may also increase the electrostatic interaction of the compound and nanocomposite surface, result in increase in degradation [18]. This interaction mainly occurred between surface of catalyst and two NH_4^+ of the Acid Blue 9. By optimizing the ratio of material in nanocomposite, in the next stage, the effect of calcination temperature on photocatalytic oxidation performance was studied. By looking into Fig. 8, the highest photocatalytic oxidation of AB9 dye was observed for 60% mol of TiO_2–SiO_2 nanocomposites prepared at 600˚C with the half-life of only 2.1 min. Very fine nanoparticles may result in fast recombination free electron and h^+ due to their abundance near surface. Therefore, 10 nm was extracted as the optimum size of pure crystalline nano-TiO_2 size with the highest photocatalytic activity [19]. Same as that statement, the best performance of nanoparticle was reported at around 9.8 nm, which was produced at 600˚C of calcination temperature. However, the study of Arai et al. [18] predicted the optimum 300˚C for the calcination temperature for reaching the best photocatalysis activity [18]. Our result stated that the nanoparticle derived at 500˚C also showed high removal rate by the half-life of 2.25 min, even though the nanoparticle size of was around 8.1 nm. Decrease the calcination temperature to around 400˚C cause dramatic decrease in efficiency of photocatalysis reaction. Complete removal of AB9 dye was expected after around 20 min using TiO_2–SiO_2 nanocomposites.

4. Conclusion

It was known that 60% TiO_2–SiO_2nanocomposites calcinated at 600˚C, indicated maximum photocatalytic activity for the AB9 dye removal. Study of crystalline structure of the synthesized nanocatalysts revealed that an increase in SiO_2–TiO_2 ratio results in thermal stability of anatase phase and grain size decrease in nanocomposites. FT-IR spectrum of the TiO_2–SiO_2 nanocomposites also confirmed the formation of Ti–O–Si bond. In addition, this increased ratio of SiO_2 to TiO_2 resulted in the increase in band gap energy followed by the increased oxidation–reduction potential of the photocatalytic. The results of BET and BJH analyses also illustrated that this increased ratio of SiO_2 to TiO_2 was due to the increase in specific surface area (leading to enhance photocatalytic activity) and decrease in the catalysts surface pore size. The optimum photocatalyst made in this study was capable of removing of AB9 dye, three times faster than available commercial nanocatalysts with the half-life of 2 min for a complex recalcitrant AB9.

References

[1] E. Forgacs, T. Cserháti, G. Oros, Removal of synthetic dyes from wastewaters: A review, Environ. Int. 30 (2004) 953–971.

[2] A. Mahyar, M. Ali Behnajady, N. Modirshahla, Characterization and photocatalytic activity of SiO_2–TiO_2 mixed oxide nanoparticles prepared by sol–gel method, Indian J. Chem., Sect. A 49 (2010) 1593–1600.

[3] H. Langhuan, W. Houjin, L. Yingliang, C. Caixuan, Preparation, characterization and photocatalytic activity of Pt-SiO_2/TiO_2 with core–shell structure, Rare Met. Mater. Eng. 40 (2011) 1901–1905.

[4] K.P.O. Mahesh, D.-H. Kuo, B.-R. Huang, M. Ujihara, T. Imae, Chemically modified polyurethane-SiO_2/TiO_2 hybrid composite film and its reusability for photocatalytic degradation of Acid Black 1 (AB 1) under UV light, Appl. Catal., A 475 (2014) 235–241.

[5] A. Srinivasan, T. Viraraghavan, Decolorization of dye wastewaters by biosorbents: A review, J. Environ. Manage. 91 (2010) 1915–1929.

[6] T. Aarthi, G. Madras, Photocatalytic degradation of rhodamine dyes with nano-TiO_2, Ind. Eng. Chem. Res. 46 (2007) 7–14.

[7] D. Beydoun, R. Amal, G. Low, S. McEvoy, Role of nanoparticles in photocatalysis, J. Nanopart. Res. 1 (1999) 439–458.

[8] X. Huang, G. Wang, M. Yang, W. Guo, H. Gao, Synthesis of polyaniline-modified Fe_3O_4/SiO_2/TiO_2 composite microspheres and their photocatalytic application, Mater. Lett. 65 (2011) 2887–2890.

[9] J. Zhang, Q. Xu, Z. Feng, M. Li, C. Li, Importance of the relationship between surface phases and photocatalytic activity of TiO_2, Angew. Chem. Int. Ed. 47 (2008) 1766–1769.

[10] T.P. Chou, Q. Zhang, G. Cao, Effects of dye loading conditions on the energy conversion efficiency of ZnO and TiO_2 dye-sensitized solar cells, J. Phys. Chem. C 111 (2007) 18804–18811.

[11] G. Balasubramanian, D.D. Dionysiou, M.T. Suidan, I. Baudin, J.-M. Laine, Evaluating the activities of immobilized TiO_2 powder films for the photocatalytic degradation of organic contaminants in water, Appl. Catal., B: Environ. 47 (2004) 73–84.

[12] C. Kapridaki, L. Pinho, M.J. Mosquera, P. Maravelaki-Kalaitzaki, Producing photoactive, transparent and hydrophobic SiO_2-crystalline TiO_2 nanocomposites at ambient conditions with application as self-cleaning coatings, Appl. Catal., B: Environ. 156–157 (2014) 416-427.

[13] R. Fateh, R. Dillert, D. Bahnemann, Preparation and characterization of transparent hydrophilic photocatalytic TiO_2/SiO_2 thin films on polycarbonate, Langmuir 29 (2013) 3730–3739.

[14] X. Zhang, Y. Zhu, X. Yang, S. Wang, J. Shen, B. Lin, C. Li, Enhanced visible light photocatalytic activity of interlayer-isolated triplex Ag–SiO_2–TiO_2 core–shell nanoparticles, Nanoscale 5 (2013) 3359–3366.

[15] Y. Hou, X. Wang, L. Wu, X. Chen, Z. Ding, X. Wang, X. Fu, N-doped SiO_2/TiO_2 mesoporous nanoparticles with enhanced photocatalytic activity under visible-light irradiation, Chemosphere 72 (2008) 414–421.

[16] T.M. Dung Dang, D. Dam Le, V. Thang Chau, M. Chien Dang, Visible-light photocatalytic activity of N/SiO_2–TiO_2 thin films on glass, Adv. Nat. Sci.: Nanosci. Nanotechnol. 1 (2010) 015004.

[17] G. Cernuto, S. Galli, F. Trudu, G.M. Colonna, N. Masciocchi, A. Cervellino, A. Guagliardi, Investigating the amorphous-crystalline interplay in SiO_2/TiO_2 nanocomposites by total scattering methods, Angew. Chem. 123 (2011) 11020–11025.

[18] Y. Arai, K. Tanaka, A.L. Khlaifat, Photocatalysis of SiO_2-loaded TiO_2, J. Mol. Catal. A: Chem. 243 (2006) 85–88.
[19] Z. Zhang, C.-C. Wang, R. Zakaria, J.Y. Ying, Role of particle size in nanocrystalline TiO_2-based photocatalysts, J. Phys. Chem. B 102 (1998) 10871–10878.
[20] M. Andersson, L. Österlund, S. Ljungström, A. Palmqvist, Preparation of nanosize anatase and rutile TiO_2 by hydrothermal treatment of microemulsions and their activity for photocatalytic wet oxidation of phenol, J. Phys. Chem. B 106 (2002) 10674–10679.
[21] L. Pinho, M.J. Mosquera, Photocatalytic activity of TiO_2–SiO_2 nanocomposites applied to buildings: Influence of particle size and loading, Appl. Catal., B: Environ. 134–135 (2013) 205–221.
[22] G. Li, R. Bai, X. Zhao, Coating of TiO_2 thin films on the surface of SiO_2 microspheres: Toward industrial photocatalysis, Ind. Eng. Chem. Res. 47 (2008) 8228–8232.
[23] A. Patterson, The Scherrer formula for X-ray particle size determination, Phys. Rev. 56 (1939) 978.
[24] N.M. Carneiro, W.C. Nunes, R.P. Borges, M. Godinho, L.E. Fernandez-Outon, W.A. Macedo, I.O. Mazali, NiO nanoparticles dispersed in mesoporous silica glass, J. Phys. Chem. C 114 (2010) 18773–18778.
[25] X. Li, J. He, Synthesis of raspberry-like SiO_2–TiO_2 nanoparticles toward antireflective and self-cleaning coatings, ACS Appl. Mater. Interfaces 5 (2013) 5282–5290.
[26] J. Liqiang, S. Xiaojun, X. Baifu, W. Baiqi, C. Weimin, F. Honggang, The preparation and characterization of La doped TiO_2 nanoparticles and their photocatalytic activity, J. Solid State Chem. 177 (2004) 3375–3382.
[27] S. Islam, R.A. Rahman, Z. Othaman, S. Riaz, M. Saeed, S. Naseem, Preparation and characterization of crack-free sol–gel based SiO_2–TiO_2 hybrid nanoparticle film, J. Sol–Gel Sci. Technol. 68 (2013) 162–168.
[28] M.R. Hoffmann, S.T. Martin, W. Choi, D.W. Bahnemann, Environmental applications of semiconductor photocatalysis, Chem. Rev. 95 (1995) 69–96.
[29] M. Kruk, M. Jaroniec, Gas adsorption characterization of ordered organic−inorganic nanocomposite materials, Chem. Mater. 13 (2001) 3169–3183.
[30] A.R. Khataee, V. Vatanpour, A.R. Amani Ghadim, Decolorization of C.I. Acid Blue 9 solution by UV/Nano-TiO_2, Fenton, Fenton-like, electro-Fenton and electrocoagulation processes: A comparative study, J. Hazard. Mater. 161 (2009) 1225–1233.